

Hidden Black: Coherent Enhancement of Absorption in Strongly-scattering Media

Y. D. Chong* and A. D. Stone

Department of Applied Physics, Yale University, New Haven, Connecticut 06520

We show that a weakly absorbing, strongly scattering (white) medium can be made very strongly absorbing at any frequency within its strong-scattering bandwidth by optimizing the input electromagnetic field. For uniform absorption, results from random matrix theory imply that the reflectivity of the medium can be suppressed by a factor $\sim (\ell_a/\ell)N^{-2}$, where N is the number of incident channels and ℓ, ℓ_a are the elastic and absorption mean free paths respectively. It is thus possible to increase absorption from a few percent to $> 99\%$. For a localized weak absorber buried in a non-absorbing scattering medium, we find a large but bounded enhancement.

PACS numbers: 42.25.Bs, 42.25.-p, 05.60.Cd

The absorption properties of a medium at a given frequency depend not only on the atomic and molecular constituents of the medium, but also on the coherence properties of the incident radiation. This was emphasized by recent work demonstrating the phenomenon of coherent perfect absorption (CPA), in which a cavity containing a weakly absorbing medium completely absorbs an appropriately-chosen input field; this is achieved by choosing the field to be the time-reverse of the lasing mode which the cavity would emit, if the loss medium were replaced by a gain medium of equal strength [1, 2]. Other input fields, differing only in the phase relationships of the incident waves, are only weakly absorbed, as are incoherent inputs. Like a laser, CPA only occurs at discrete frequencies in a given system. This raises a question: under what conditions, if any, is it possible to control absorption over a continuous and large frequency range by optimizing the input fields at each frequency?

A related question, which has recently been extensively studied, concerns the conditions under which light can be transmitted through an opaque, *lossless*, multiple-scattering medium. In the diffusive regime, the transmission probability decays as ℓ/L , where ℓ is the elastic transport mean free path and L is the sample length; hence a sample with $L \gg \ell$ is highly reflecting at all frequencies. Nonetheless, it has been known for some time that at any frequency there do exist coherent superpositions of input fields which penetrate much further than the mean free path, and hence may transmit with high probability through the sample [3–6]. This effect has been demonstrated experimentally in the past few years, as practical methods were found for determining the optimal input fields without detailed *a priori* knowledge of the scattering configuration [7, 8]. This suggests that if a multiple-scattering medium contains some material absorption, then even if that absorption is weak (i.e., the medium normally appears “white”), it should be possible to substantially enhance the *effective* absorption at any frequency within a wide and continuous frequency range, by tuning the input fields to penetrate deeply enough that the photon path length exceeds the large but finite absorption length. In this Letter, we provide a theoretic

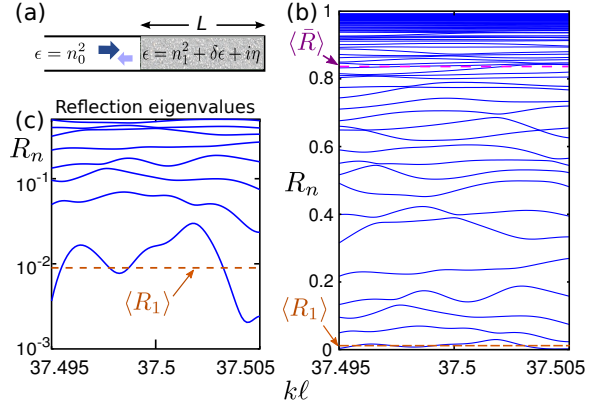


FIG. 1: (color online) (a) Model of an absorptive multiple-scattering system. A waveguide with dielectric constant n_0^2 is connected to a region of length L with dielectric $n_1^2 + \delta\epsilon + i\eta$, where $\delta\epsilon(x)$ is a real white-noise disorder term drawn from a uniform distribution over $[-d_0, d_0]$, and η is the material absorption. (b) Variation of reflection eigenvalues $\{R_n\}$ with frequency k for a fixed disorder realization, with $n_0 = n_1 = 1.5$, $N = 80$ scattering channels, mean free path $\ell = 0.05L$, and uniform η with ballistic absorption length $\ell_a = 13.3L$. Dashed lines show the ensemble averages of the mean and smallest reflectivity, \bar{R} and R_1 . (c) Semi-log plot of R_1 , which fluctuates, but is $\sim 10^{-2}$ over a continuous frequency range.

cal and numerical demonstration of this effect, which we refer to as *coherently enhanced absorption* (CEA). It is in general distinct from CPA, which follows rigorously from time-reversal symmetry and is not specific to multiple scattering media (but requires fine-tuning of the sample parameters and operating frequency).

Linear scattering from a medium is described by the scattering matrix (S-matrix), which relates incident and scattered amplitudes in the basis of asymptotic free solutions of the wave equation. The S-matrix depends on the scattering geometry and material properties, as well as the frequency of the input fields, but does not depend on the fields themselves. Given a vector $|\psi_{\text{in}}\rangle$ whose components are the intensity-normalized input amplitudes in each of the N scattering channels, the output amplitudes are $|\psi_{\text{out}}\rangle = S|\psi_{\text{in}}\rangle$, and the total output intensity

is $\langle \psi_{\text{out}} | \psi_{\text{out}} \rangle = \langle \psi_{\text{in}} | S^\dagger S | \psi_{\text{in}} \rangle$. For a lossless system, this quantity is always unity since S is unitary; in the presence of absorption, it is smaller than one [9].

We will focus on the case of scattering from one surface of an optically dense and weakly absorbing medium, in which all incident fields are either reflected or absorbed, so that the S-matrix coincides with the reflection matrix r . Denote the eigenvalues of the Hermitian matrix $r^\dagger r$ by R_n , where $0 \leq R_1 \leq \dots \leq R_N < 1$. The sample-specific “mean reflectivity” $\bar{R} = (1/N) \sum_n R_n$ is the normalized output power when the inputs in each channel are independent (e.g. having no coherent phase relationship); the moments of this quantity were studied in earlier works on reflection from random absorbing media [10, 11]. In studying CEA, the relevant physical quantity is the *smallest* reflection eigenvalue, R_1 . By the variational principle, $\langle \psi_{\text{in}} | r^\dagger r | \psi_{\text{in}} \rangle \geq R_1$ for any intensity-normalized $|\psi_{\text{in}}\rangle$. Hence, $1 - R_1$ is the maximum amount of absorption that can be achieved, and its eigenvector gives the maximally-absorbed set of input amplitudes. In an experiment, if noise sources rule out measuring reflectivities below a value $R' > R_n$, any input waveform in the eigenspace spanned by eigenvectors of $R_1, R_2 \dots R_n$ will give reflectivity $\sim R'$. However, we note that enhanced absorption can also be measured directly, e.g. via fluorescence or heat generation.

We employ a model previously introduced and studied by Beenakker *et al.* [10], and by Bruce and Chalker [11]. As shown in Fig. 1(a), it consists of a waveguide with N channels, containing a medium with elastic scattering mean free path ℓ and ballistic absorption length ℓ_a . The ratio of these lengths defines the absorption parameter $a \equiv \ell/\ell_a$, with $a \ll 1$ in the regime of interest. In addition, the quantity $L_a \equiv \sqrt{\ell_a \ell}$ gives the average distance a diffusing particle penetrates into the medium before being absorbed. From the combination law for infinitesimal scattering segments (each of which randomly scatters between channels and also imposes some absorption parameterized by a), the joint probability distribution (JPD) for the reflection eigenvalues can be shown to evolve with the sample length L according to the equation [10, 11]

$$\ell(N+1) \frac{\partial p_x}{\partial L} = \frac{1}{2} \sum_n \frac{\partial^2 p_x}{\partial x_n^2} + \frac{1}{2} \sum_n \frac{\partial}{\partial x_n} \left(\frac{\partial V}{\partial x_n} p_x \right), \quad (1)$$

where $p_x(\{x_n\})$ is the JPD given in terms of the variables $x_n \equiv \frac{1}{2} \cosh^{-1}[(1 + R_n)/(1 - R_n)]$. This change of variables leaves the diffusion term in (1) independent of $\{x_n\}$, allowing analytic solution of the stationary distribution. The “potential” V in Eq. (1) is given by

$$V = \sum_n \left[a(N+1) \cosh(2x_n) - \ln |\sinh(2x_n)| \right] - \sum_{m>n} \ln [\cosh(2x_m) - \cosh(2x_n)]. \quad (2)$$

Eq. (1) is similar to the Dorokhov-Mello-Pereyra-Kumar (DMPK) diffusion equation [12, 13], which is derived from a quasi-one-dimensional (quasi-1D) waveguide model without absorption. The DMPK equation describes the JPD of transmission and reflection eigenvalues, and its results have been found to generalize to geometries with no transverse confinement, as when a surface is illuminated by a spot [14] (the geometry used in subsequent experiments on coherently enhanced transmission [7]). We expect the results for the absorbing case to generalize in the same way.

For $L_a < L$, $p_x(x_1, \dots, x_N) \sim e^{-V}$ is the stationary (L -independent) limiting solution to (1). To make contact with standard random matrix theory (RMT), a further change of variables $y_n \equiv 2a(N+1)[\cosh(2x_n) - 1]$ is performed, which yields

$$p_y(y_1, \dots, y_N) \sim e^{-\frac{1}{2} \sum_n y_n} \prod_{m>n} (y_m - y_n). \quad (3)$$

This is the Laguerre eigenvalue distribution, characteristic of a well-studied ensemble in RMT [15]. The ensemble-averaged mean reflectivity can be determined by integrating over this distribution [10, 11]:

$$\langle \bar{R} \rangle \approx 1 + 2a - 2\sqrt{a(1+a)}. \quad (4)$$

Note that this result is independent of N .

We are interested in the distribution of the smallest reflection eigenvalue, R_1 . This can be found from the fact that Ny_1 follows a χ_2^2 distribution [15]. Thus,

$$p(R_1) = 2aN(N+1) \frac{e^{-2aN(N+1) \frac{R_1}{1-R_1}}}{(1-R_1)^2}, \quad (5)$$

and the ensemble-averaged value is

$$\begin{aligned} \langle R_1 \rangle &= 1 + 2aN(N+1) e^{2aN(N+1)} \text{Ei}[-2aN(N+1)] \\ &\approx [2aN(N+1)]^{-1} \text{ for } a \gtrsim N^{-3/2}. \end{aligned} \quad (6)$$

Unlike $\langle \bar{R} \rangle$, this quantity *does* depend on N . The decrease of R_1 with increasing N is very natural, because the eigenvalue repulsion characteristic of RMT ensembles tends to push the smallest eigenvalue to small values.

Thus, even if the material absorptivity is weak enough that $\langle \bar{R} \rangle \sim 1$, if N is sufficiently large then $R_1 \sim 1/aN^2$ can be very small. In typical free-space optical experiments $N \approx A/\lambda^2$ where A is the spot size, so this condition should be easily achieved. According to (4) and (6), the regime of weak average absorption and strong optimal absorption is $a \ll 1 \ll 2aN^2$. The physical interpretation of these inequalities is that photons have little chance of being absorbed between scattering events ($\ell_a \gg \ell$), but those in the maximally-absorbed mode have a negligible chance of diffusing the entire quasi-1D localization length $\xi = N\ell$ before being absorbed. For example, for $a \leq 0.01$ and $N = 80$, we have $\langle \bar{R} \rangle \geq 0.8$ and $\langle \bar{R}_1 \rangle < 0.01$.

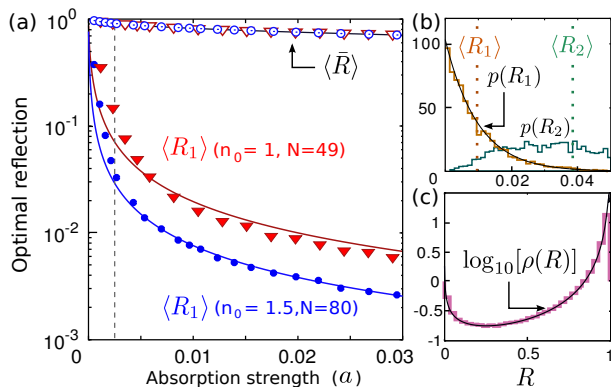


FIG. 2: (color online) (a) Mean reflectivity \bar{R} (open symbols) and smallest reflection eigenvalue R_1 (filled symbols) vs the absorption strength a . Each data point is an average over 2000 disorder realizations. The scattering medium has $n_1 = 1.5$, disorder strength $d_0 = 0.6$ ($\ell = 0.05L$), and uniform absorption. Two simulation sets are shown: (i) external index $n_0 = 1.5$ and $N = 80$ exterior waveguide channels (circles); and (ii) index mismatch with $n_0 = 1$ and $N = 49$ exterior channels (triangles). In each case, we fit $\langle \bar{R} \rangle$ to Eq. (4) to obtain the constant c_0 in $\ell_a^{-1} = c_0 \eta k / 2n_1$, finding $c_0 = 2.14$ for (i) and $c_0 = 4.65$ for (ii). This determines the analytic form of $\langle R_1 \rangle$, plotted as solid curves, with no free parameters. The vertical dashed line denotes $a \geq (\ell/L)^2$, required for the stationary solution to apply. (b) Distributions of R_1 and R_2 from simulations (histograms). The solid line shows the analytical expression (5) for $p(R_1)$; dotted lines show the ensemble averages $\langle R_1 \rangle$ and $\langle R_2 \rangle$. (c) Semi-log plot of reflection eigenvalue density, comparing simulations (histogram) to the approximate density $2a(N+1)\sqrt{[N(1-R)/a(N+1)R] - 1/\pi(1-R)^2}$ (solid line), from the large- N density of the Laguerre distribution [15]. The simulations for (b) and (c) were performed with $n_0 = 1.5$ ($N = 80$) and $\eta = 0.0003$ ($\ell_a = 125\ell$).

To test and generalize the above results, we have performed numerical simulations of scalar wave propagation in quasi-1D structures. The wave equation $(\nabla^2 + \epsilon k^2)\psi = 0$ is discretized using a 2D tight-binding model on a square grid. A semi-infinite uniform waveguide of index n_0 is connected to a scattering region with average index n_1 , uniform absorption η and random scatterers; see Fig. 1(a). The reflection matrix is computed for this rectangular region, of varying length and width and perfectly reflecting walls on three sides, using the recursive Green's function method [10, 16]. The elastic mean free path ℓ is computed using the relation $\langle \bar{T} \rangle \equiv \ell/L$, via separate transmission simulations without absorption. In all simulations, we use frequency $k = 750/L$, lattice spacing $L/750$, and waveguide width $L/5$. The ballistic absorption length is $\ell_a^{-1} = c_0 \eta k / 2n_1$, where c_0 is a constant of order unity determined by a fit to Eq. (4).

The variation of $\langle \bar{R} \rangle$ and $\langle R_1 \rangle$ with ℓ/ℓ_a is shown in Fig. 2(a), together with the analytic predictions. Two sets of simulations are plotted. In the first, the lead and scattering medium are index-matched ($n_0 = n_1 = 1.5$)

as in the model of [10, 11]. In the second, they are mismatched with $n_0 = 1$, $n_1 = 1.5$, representing scattering from air into a denser medium, a case for which analytic results were not known. In both cases, despite weak average absorption ($\ell_a > 40\ell$ and $\langle \bar{R} \rangle \sim 1$), we obtain values of $\langle R_1 \rangle$ as small as 10^{-2} to 10^{-3} . For the index-matched results the data for $\langle R_1 \rangle$ agree very well with the theory, Eq. (6), using the number of exterior channels, $N = 80$. For the index-mismatched case, the exterior waveguide has fewer channels, $N = 49$, at the same frequency, compared to the average of 80 interior channels; nonetheless, we find that Eq. (6) holds very well using the exterior channel number. Thus, illuminating from a lower index medium (e.g. from air) does diminish the CEA effect compared to the index-matched case, but large enhancement is still possible and is governed by the same factor of $(2aN^2)^{-1}$. Figs. 2(b) and (c) show the numerical distributions of the reflection eigenvalues for fixed a , which are in excellent agreement with the theoretical distributions. The distribution of R_2 in Fig. 2(b) illustrates the role of eigenvalue repulsion in confining R_1 to small values.

The analytic predictions for $\langle R_1 \rangle$ and $\langle \bar{R} \rangle$ have no dependence on the frequency k , apart from the weak variation of the number of exterior channels N with k , assuming that the parameter a varies negligibly with frequency. Unlike the CPA systems studied in Refs. [1, 2], in which near-perfect absorption is obtained at particular discrete values of a and k , in the present systems highly enhanced absorption is possible at any frequency *so long as the incident waveform is optimized in the vicinity of each frequency of interest*. Thus, while CEA is not a broadband effect in the usual sense, it can be realized over a wide range of frequencies. To determine the frequency interval over which a fixed waveform, optimized at a single frequency, will still lead to strongly enhanced absorption, we calculate the frequency correlation of R_1 , shown in Fig. 3. We find that the decorrelation frequency scale is $k_c \approx 0.5/\ell_a$, which is to be expected; by analogy to the case of transmission through a non-absorbing medium, where the decorrelation scale is determined by the length of paths that traverse the sample and escape, here the maximally-absorbed mode arises from the interference of many coherent paths of length $\sim \ell_a$. Thus, measurements obtained at frequency intervals $\Delta k \gg 0.5/\ell_a$ are independent. For $\ell = 1\mu\text{m}$, $\ell_a = 100\ell$, and $\lambda = 1.5\mu\text{m}$, this gives $\Delta\lambda_c \approx 1.5\text{nm}$. While the CEA effect is more robust than CPA when $N \gg 1$, it should be noted that, when $N \rightarrow 1$, continuous CEA is no longer possible, whereas CPA can still occur at discrete frequencies.

An interesting and important extension of the above model is to a localized or extended absorber buried behind a layer of lossless scattering medium. Such a system has been studied experimentally by Vellekoop *et al.*, who demonstrated strong focusing of light through a lossless medium to enhance fluorescence in a small interior spot [17]. To our knowledge, there has been no theoretical

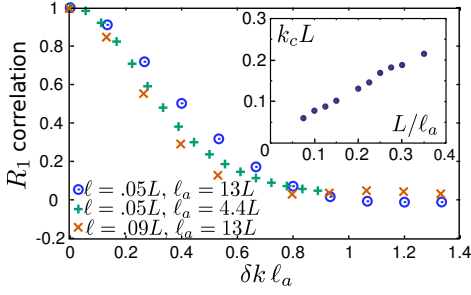


FIG. 3: (color online) Normalized correlation function for the smallest reflection eigenvalue R_1 , defined as $C_{R_1}(\delta k) \propto [\langle R_1(k + \delta k) R_1(k) \rangle - \langle R_1(k) \rangle^2]$ with $C_{R_1}(0) = 1$. Each data set consists of 3000 disorder realizations. Inset: plot showing the linear dependence on $1/\ell_a$ of the decorrelation frequency k_c , defined by $k_c \equiv C_{R_1}(k_c/2) = 1/2$. Here, $\ell = 0.05L$.

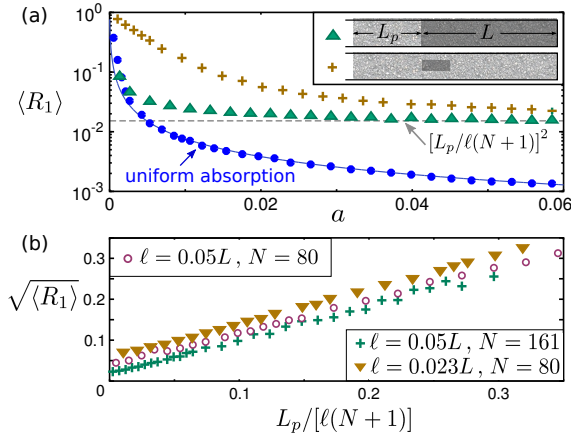


FIG. 4: (color online) (a) Variation of R_1 with a for buried absorbers. In the first set of simulations (triangles), the absorbing region (length L , width $0.2L$ equal to the waveguide width, and $\ell = 0.05L$) lies behind a segment of lossless scattering material (length $L_p = 10\ell$, with the same ℓ). In the second set of simulations (crosses), the absorbing region has dimensions $0.06L \times 0.08L$ and is surrounded by the lossless medium. The uniform absorption case, similar to Fig. 2, is shown for comparison (circles). (b) Plot of $\sqrt{\langle R_1 \rangle}$ vs the Fokker-Planck “time” $L_p/\ell(N+1)$, for the full-width absorber with $a = 0.04$. Note that $R_n \approx x_n^2$, where x_n are the variables of Eq. (1).

work on the limiting efficiency of such a process. We consider two variant models, shown in the inset of Fig. 4(a). A lossless region of length L_p is added in front of the absorbing region of length L , which contains either uniform absorption or a localized absorber. For a within the absorber satisfying $2aN^2 \gg 1$, the simulations still show CEA of approximately two orders of magnitude. However, R_1 now saturates with increasing a to a value $\approx (L_p/\ell N)^2$. This saturation value appears to be independent of the size of the absorbing region, though the larger region reaches this value for smaller a .

To understand this behavior qualitatively, we return to Eq. (1)-(2). One can think of the eigenvalues $\{x_n\}$ as

interacting gas particles with a stationary distribution at length L , in which the confining potential due to a in (2) is balanced by diffusion and interparticle interactions [6]. This is the distribution for which $\langle R_1 \rangle \approx (2aN^2)^{-1}$ for the extremal particle. Adding the lossless region corresponds to turning off the confining potential for a “time” $T = L_p/\ell(N+1)$, causing the particles to drift and diffuse to larger values of x_n . In fact, Fig. 4(b) shows that $\langle x_1(L_p) \rangle \sim T$, so that $\langle R_1 \rangle \approx \langle x_1^2 \rangle \sim T^2$, which is the saturation scale observed in Fig. 4(a). For $L_p \lesssim \ell(N+1)$, these results show the feasibility of enhancing the delivery of energy to a buried absorber by orders of magnitude.

A final critical question is whether incident waveforms approaching the CEA optimum can be found when details of the scattering medium are unknown, via an empirical optimization scheme analogous to those employed for transmission through lossless media [7, 8]. Initial numerical tests based on our model are promising, with simple optimization schemes giving order of magnitude increases in absorption, though not yet approaching theoretical limits. This problem, and that of the buried absorber, are rich and exciting directions for future work.

This work was partially supported by NSF Grant No. DMR-0908437, by seed funding from the Yale NSF-MRSEC (DMR-0520495), and by the facilities and staff of the Yale University Faculty of Arts and Sciences High Performance Computing Center. We thank Hui Cao and Wenjie Wan for helpful discussions.

* Electronic address: yidong.chong@yale.edu

- [1] Y. D. Chong, Li Ge, Hui Cao, and A. D. Stone, Phys. Rev. Lett. **105**, 053901 (2010).
- [2] W. Wan, Y. D. Chong, Li Ge, Heeso Noh, A. D. Stone, and Hui Cao, Science **331**, 889 (2011).
- [3] O. N. Dorokhov, Solid State Commun. **51**, 381 (1984).
- [4] Y. Imry, Europhys. Lett. **1**, 249 (1986).
- [5] J. B. Pendry, A. MacKinnon, and A. B. Pretre, Physica (Amsterdam) **168A**, 400 (1990).
- [6] C. W. J. Beenakker, Rev. Mod. Phys. **69**, 731 (1997).
- [7] I. M. Vellekoop and A. P. Mosk, Opt. Lett. **32**, 2309 (2007); Phys. Rev. Lett. **101**, 120601 (2008).
- [8] S. M. Popoff *et al.*, Phys. Rev. Lett. **104**, 100601 (2010).
- [9] C. W. J. Beenakker, Phys. Rev. Lett. **81**, 1829 (1998).
- [10] C. W. J. Beenakker, J. C. J. Paasschens, and P. W. Brouwer, Phys. Rev. Lett. **76**, 1368 (1996).
- [11] N. A. Bruce and J. T. Chalker, J. Phys. A Math. Gen. **29**, 3761 (1996).
- [12] O. N. Dorokhov, JETP Lett. **36**, 318 (1982).
- [13] P. A. Mello, P. Pereyra, and N. Kumar, Ann. Phys. (N.Y.) **181**, 290 (1988).
- [14] Yu. V. Nazarov, Phys. Rev. Lett. **73**, 134 (1994).
- [15] A. Edelman, SIAM J. Matrix Anal. Appl. **9**, 543 (1988).
- [16] P. A. Lee and D. S. Fisher, Phys. Rev. Lett. **47**, 882 (1981).
- [17] I. M. Vellekoop, E. G. van Putten, A. Lagendijk, and A. P. Mosk, Opt. Ex. **16**, 67 (2008).